Hindawi
Advances in Civil Engineering
Volume 2020, Article ID 8863645, 13 pages
https://doi.org/10.1155/2020/8863645

Research Article

Analysis of the Damage Characteristics and Energy Dissipation of Rocks with a Vertical Hole under Cyclic Impact Loads

Bing Dai,[1,2,3] **Xinyao Luo**,[1] **Li Chen**,[2] **Yakun Tian**,[1] **Zhijun Zhang**,[1,3] **Ying Chen**,[1,3] **and Qiwei Shan**[1]

[1]*School of Resources Environment and Safety Engineering, University of South China, Hengyang, China*
[2]*Deep Mining Laboratory of Gold Group Co., Ltd, Laizhou, China*
[3]*Hunan Province Engineering Technology, Research Center for Disaster Prediction and Control on Mining Geotechnical Engineering, 421001 Hengyang, China*

Correspondence should be addressed to Yakun Tian; 1090596259@qq.com and Ying Chen; csu_chenying@csu.edu.cn

Received 16 April 2020; Revised 18 May 2020; Accepted 22 May 2020; Published 22 July 2020

Academic Editor: Hailing Kong

This study systematically investigates the failure patterns, energy dissipation, and fracture behavior of rock specimens containing a vertical hole under impact loads. First, an improved damage calculation equation suitable for the analysis of rock specimens with a vertical hole is obtained based on the one-dimensional stress wave theory and the interface continuity condition. After that, the Hopkinson pressure bar (SHPB) device was used to conduct cyclic impact tests with different impact pressures and impact modes (impact pressures with equal amplitude and unequal amplitude). The experimental results suggest that, under the equal-amplitude high pressure and unequal-amplitude pressure, the degree of damage of the rock significantly increased, the bearing capacity greatly reduced, and the rock gradually transitions from having good ductility to experiencing brittle failure. The cumulative specific energy absorption value gradually increases with the increase in the cyclic impact. Compared to that of the equal impact condition, the degree of damage to the rock is more severe for the case of equal-amplitude high pressure and unequal impact, and the failure mode undergoes a transformation from transverse tensile failure to transverse tensile failure-axial splitting failure combination and axial splitting failure. Through the analysis of rock energy changes and rock failure patterns during cyclic impact, it will be helpful to predict and control the fracture caused by local stress concentration during excavation, thus can reduce the cost of support and reinforcement in excavation and improve the stability of surrounding rocks.

1. Introduction

Unexpected swift increases in urbanization throughout the world have brought the demand for more land and faster transportation between cities or intercity. In order to keep pace with the demand, more and more underground engineering, highways, and railways are under construction [1–3]. In these constructions, it is unavoidable to encounter the excavation work. Blast and mechanical excavations are the usual way to accomplish this process. As the main medium in various underground projects, rock is inevitably subjected to dynamic loads, such as mechanical drilling and blasting, during the construction of a tunnel or city underground engineering, which causes the internal structure and energy of the surrounding rocks to change, and long-term accumulation will cause hidden safety risks.

Therefore, many scholars have performed substantial research on the dynamic mechanical properties, damage, and energy dissipation of rocks under dynamic loads [4–6]. Zhu et al. [7] used a large-diameter SHPB device to conduct cyclic impact tests, analyzed the mechanical characteristics and energy absorption trends of granite, and obtained a damage model based on the Weibull distribution. Gong et al. [8] used a modified triaxial SHPB system to analyze the relationship between high strain rate, low yield pressure, and the dynamic mechanical properties of sandstone. Shu et al. [9] heat treated granite under a cyclic impact load test and obtained the relationship between the rock energy and

failure patterns with the temperature. Peng et al. [10, 11] revealed the effects of confining pressure on physical quantities, such as the stress-strain and damage factor, by using different confining pressures for tests on sandstone and gained the relationship among the strain rate, energy, and damage degree. Tao et al. [12] studied the dynamic failure process of granodiorite rock including an elliptical hole, and the results indicated that the elliptical hole in rock may lead to obvious stress concentration and energy accumulation which can cause considerable decreases in the strength parameters.

In the practical underground engineering, undisturbed rock mass encompasses various defects such as fissures, joints, weak surfaces, pores, and cavities [13]. The instability and failure of a rock mass usually begins with initial defects, such as holes and fissures. At present, there are few reports on studies of rock with defects under dynamic loading. Zhou [14, 15] analyzed the crack propagation and failure process of prefabricated cracks and holes in layered sandstone and marble, respectively, by using a high-speed camera and described the effects of the crack inclination, hole shape, and size on the dynamic compressive strength. Li et al. [16] carried out experiments on prismatic marble specimens containing a single flaw using a modified SPHB and revealed that the geometry of the flaws may have a slight effect on the failure modes of flawed rock under impact loading. Tao et al. [17] prefabricated round holes in granite and observed the failure process of the specimen under different combinations of static and dynamic stress with a high-speed camera. Based on the true triaxial static load and vertical dynamic load, Liu et al. [18] carried out rock burst tests on the sandstone samples with holes in the center and compared and analyzed the characteristics of fragments and energy dissipation after failure obtained by the two loading methods. Wu et al. [19] analyzed the fracture morphology on the axial surface by using the SHPB device, and the results showed that the energy absorption rate and energy consumption density decrease firstly and then increase.

In the cumulative process of damage under cyclic dynamic loads, the mechanical properties of the rock become gradually degraded, the ability to withstand external dynamic load becomes lower, and the integrity becomes worse. In addition, the original rock stress further aggravates the damage of the rock, resulting in the reduction of the bearing capacity and stability of the rock mass. Therefore, rock damage under dynamic loading and its evolution law are the important research topics in rock dynamics. The methods for defining rock mass damage variables include elastic modulus method, ultrasonic wave velocity method, density and gravity method, energy method, strain method [20], CT method, and acoustic emission cumulative number method [21]. In addition, many scholars have derived constitutive models which were suitable for defining the rock mass damage through research. Zhu et al. [22] proposed a linear damage model for rock mass based on cyclic loading times and fatigue life, but its accuracy was far from the actual situation. Based on the deformation characteristics of rocks under cyclic loading, Zheng et al. [23] established a fatigue damage model related to failure factors under triaxial cyclic loading, which could be applied to engineering practice. Meng et al. [24] established a dynamic statistical damage constitutive model under Weibull distribution, which was suitable for dynamic load conditions, and its calculation curve was in good agreement with the test curve. Wu et al. [25] proposed a quantitative method of rock impact fatigue performance for the engineering application under repeated blasting. Chen et al. [26] selected different damage variables from different perspectives with respect to the random distribution of microscopic unit strength of rocks and established two damage constitutive models subject to lognormal distribution, which were effectively proved by triaxial compression test data.

With respect to the rock with various defects, research on prefabricated cavity rocks in the energy and damage fields is also very important. Zhou et al. [27] tested the marble specimens with single or two rectangular holes in different layouts under uniaxial compression and revealed the relationship between absorption energy per unit volume and the degree of crushing of the specimens. Based on the theory of particle discrete element, Scholtès and Donzé [28] carried out numerical simulation of compression failure process of tuffaceous sandstone with holes under the conditions of uniaxial, biaxial, and triaxial, and the results showed that the strain energy and dissipation could reflect the rock destruction process and degree of the sliding and friction of the mesoscopic particles. Liu et al. [18] conducted true triaxial static load and vertical dynamic load rockburst tests on sandstone samples with central hole, analyzed the relationship between the number of debris particles and energy dissipation, and concluded that the energy dissipation of the rockburst test was greater than that of the uniaxial compression test. In terms of damage research, Matvienko et al. [29] used electronic speckle interferometry (ESPI) to measure the deformation response of local materials caused by hole defects under low-period fatigue load and proposed and verified a new method for quantitative determination of damage accumulation in the stress concentration area.

As shown in Figure 1, in previous research on the dynamic characteristics of rock with holes, transverse holes were prefabricated in the vertical direction of the dynamic load. Few scholars have studied the damage accumulation and energy dissipation of vertical hole rocks distributed in the direction of the dynamic load. In the study of rock failure mechanism in underground excavation engineering, rocks are usually divided into two types. The first type regards the hole as the excavation cavern, such as tunnel [30] and chamber [31]. The second type regards the hole as the initial defect inside the rocks [17, 18]. If the hole is regarded as a cavern, the transverse hole and the vertical hole can be regarded as the propagation of stress wave on the hole plane and the propagation on the vertical hole plane. If the hole is regarded as the initial defect, the difference between them is the distribution in the rocks relative to the stress wave propagation direction. The disturbance of two-way excavation in tunnel engineering usually acts in the direction of the hole. When the two-way excavation of the tunnel is close to penetration, the drilling and blasting of the tunnel on one side greatly affects the stability of the surrounding rock of the

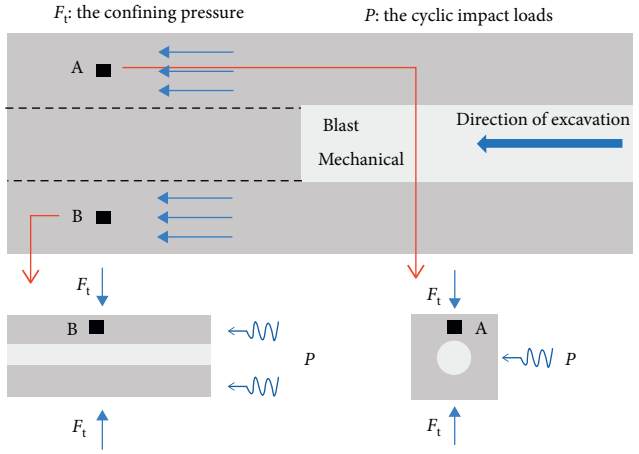

Figure 1: Sketch of rock mass subjected to cyclic dynamic loads in excavation.

tunnel on the other side. The impact load generated by actual drilling and blasting often varies [32]. Therefore, this article will use a SHPB device to carry out cyclic impact tests of equal and unequal pressures on granite with vertical holes, compare and analyze the cumulative damage and energy dissipation characteristics of rock samples, and explore the response characteristics of rocks under different pressure impacts. A theoretical reference will also be provided for correctly understanding the granite failure mechanism and the engineering confining pressure stability under actual conditions.

2. Methodology: Establishment of the Damage Model

Jiefang et al. [33] deduced the expression for wave impedance from incident waves, reflected waves, and transmitted waves based on one-dimensional stress wave theory. The results show that the damage variables defined based on the wave impedance exist in the rock fatigue mechanical properties from the initial stage to the low-speed stage and the acceleration stage, which have the same trend as the damage variables defined by the P-wave velocity. Therefore, the wave impedance of the specimen is used to define the change in the damage to the rock in this cyclic impact test. The degree of damage D to the specimen can be expressed as

$$D = 1 - \left(\frac{\overline{\rho C}}{\rho C}\right)^{1.6}, \tag{1}$$

where $\overline{\rho C}$ is the wave impedance in a certain damage state of the rock and ρC is the wave impedance in the initial state of the rock. The vertical hole is prefabricated in the center of the cylindrical rock sample in this test, so the cross-sectional areas of the elastic rod and the test specimen are not equal. The equation for calculating the wave impedance derived by Jin cannot be directly applied to this experiment. It is assumed that the contact surface between the rock and the elastic rod is a two-elastic half-space contact surface with displacement discontinuity. At this time, the propagation of the stress wave at the contact surface can be transformed to solve the boundary value problem of the wave equation.

As shown in Figure 2, when the stress wave enters the specimen from the rod part, the wave resistance changes from m_t to m_s at the interface according to the one-dimensional stress wave theory [34]. The continuous condition on I-II has the following equations:

$$P_R = \lambda P_I, \tag{2}$$

$$P'_T = (1-\lambda)P_I, \tag{3}$$

$$m_t = \rho_t C_t A_t, \tag{4}$$

$$m_s = \rho_s C_s A_s, \tag{5}$$

$$\lambda = \frac{m_t - m_s}{m_t + m_s}, \tag{6}$$

where P_I, P_R, and P'_T are the incident wave, reflected wave, and transmitted wave in the specimen, respectively; A_t, A_s, ρ_t, ρ_s, C_t, and C_s are the cross-sectional area, density, and P-wave velocity of the elastic rod and the specimen, respectively; and λ is the reflectance of the one-dimensional longitudinal wave when it enters the specimen from the incident rod.

In actual experiments, since the reflected wave and the incident wave are measured by the same strain gauge, the incident wave may still be present when the reflected wave is present, and then the starting point of the reflected wave will be greatly affected by the incident wave. At this time, the corresponding time is difficult to be determined, which can cause data errors, but the starting point of the transmitted wave will not be disturbed by the incident wave, so equation (3) can be used to derive the damage model. Then, the incident wave and the transmitted wave are functions of time, and equation (3) is transformed into a continuous condition on interface III-IV to obtain the following equation:

$$\sigma_T(t_i) = \left(1-\lambda^2\right)\sigma_I(t_i). \tag{7}$$

Knowing the wave impedance of the elastic rod and the rock specimen, the time relationship between the wave impedance and the wave can be obtained by combining equations (6) and (7):

$$f(t_i) = \frac{\sigma_T(t_i)}{\sigma_I(t_i)} = \frac{4m_t m_s}{(m_t + m_s)^2}, \tag{8}$$

where $\sigma_I t_i$ and $\sigma_T t_i$ are the incident wave and transmission wave of the i-th impact wave, respectively, and $f(t_i)$ is the ratio of the i-th shock transmitted wave to the incident wave. By bringing equations (4) and (5) into equation (8) and solving the root of the quadratic equation by the inverse function transformation and global substitution, the effective expression of the wave impedance of the rock specimen at the i-th impact at a certain moment can be obtained:

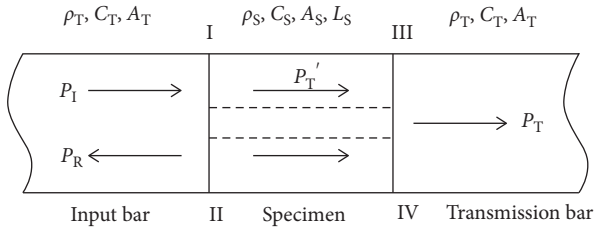

Figure 2: Transmission and reflection of the one-dimensional longitudinal wave in the specimen.

$$\rho_i C_i = \zeta \frac{2 - f(t_i) - 2\sqrt{1 - f(t_i)}}{f(t_i)} \rho_t C_t, \tag{9}$$

$$\zeta = \frac{A_s}{A_t}. \tag{10}$$

The following expression of rock damage can be obtained by substituting equation (9) into equation (1):

$$D = 1 - \left(\zeta \frac{2 - f(t_i) - 2\sqrt{1 - f(t_i)}}{f(t_i)} \frac{\rho_t C_t}{\rho C} \right)^{1.6}, \tag{11}$$

where $\rho_i C_i$ is the wave impedance value of the i-th impact rock specimen and ζ is the cross-section proportionality coefficient between the specimen and the elastic rod. In this test, the average diameter of the granite section is $\overline{D} = 4.85$ cm, and the average diameter of the pores is $\overline{d} = 1.10$ cm. The result is $\overline{\zeta} = 0.8925$. Since one impact of the specimen is the result of incident and multiple reflections, the wave impedance value of the rock specimen is always changing throughout the process. Li [33, 35] pointed out that when $t \le (2L_s/C_s)$, the measured reflected and transmitted waves will not be affected by secondary and more reflections and transmissions, and the wave impedance change trend is relatively gentle during this period. Figure 3 shows the relationship between the wave impedance and time when D-0.6-1 is impacted. It can be seen from the figure that there is a relatively stable area of wave impedance after point A, and it has a similar slope of change. After point B, a downward trend begins. At this time, the fissures inside the rock initiate and further expand. Therefore, a point on AB in the $(0, 2L_s/C_s)$ time section is selected as the fixed time point for the calculation of the wave impedance.

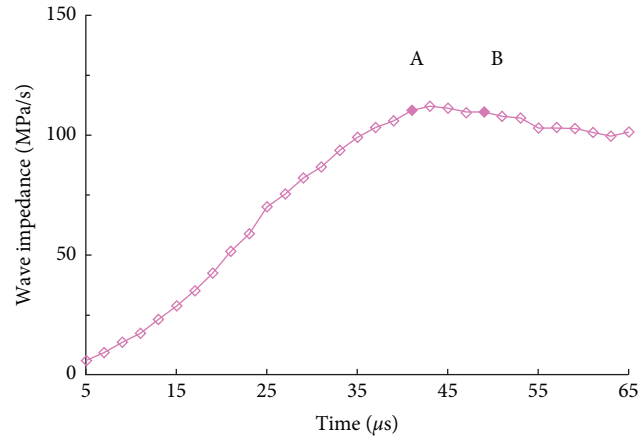

Figure 3: The trend of the wave impedance of the specimen over time.

3. Experimental Design

3.1. Sample Preparation. The rock sample is granite with good integrity and homogeneity, with a density of 2790 kg/m^3, a P-wave velocity of 5345 m/s, and an elastic modulus of approximately 40.7 GPa. Figure 4 shows a prefabricated granite specimen with vertical holes. The test specimen is made into a cylindrical rock sample with a growth diameter ratio of 2 : 1, a size of ϕ50 mm × 100 mm, and a vertical hole in the center of the circular cross section with a diameter of 10 mm. Before testing, the two ends and sides of the specimen are carefully polished to ensure that their nonparallelism and nonverticality are less than 0.02 mm. High-pressure water cutting technology is used to precast vertical holes in the center of the circular cross section of the specimen with a water jet cutting machine to avoid mechanical damage to the rock sample body caused by the process of smoothing the hole surface.

3.2. Experimental Equipment. The test equipment is a 50 mm diameter Hopkinson pressure bar (SHPB) device from Central South University. The punch, incident rod, transmission rod, and absorption rod of the device are made of 40Cr alloy steel. The longitudinal wave velocity is 5400 m/s, the density is 7810 kg/m^3, the elastic modulus is 240 GPa, and the wave impedance is 4.2 × 107 MPa/s. Two sets of strain gauges are attached to the incident rod and the transmission rod, and the deformation of the rod is collected and displayed with the help of a CS-1D superdynamic strain gauge and a DL-750 oscilloscope. In the launch cavity, PC vibration is eliminated to achieve half-sine wave loading, thereby achieving a constant strain rate loading. Figure 5 shows a schematic diagram of the SHPB test system and testing equipment.

3.3. Experimental Plan

3.3.1. The Method. To study the law and to compare the strain damage and energy dissipation of granite under cyclic impact with equal amplitude and cyclic impact with unequal amplitude, the impact air pressure was set to 0.6 MPa, 0.7 MPa, and 0.8 MPa for cyclic impact. The cyclic effects of varying loads on the rock mass during blasting were simulated using impact pressures of 0.6–0.7 MPa and 0.7–0.8 MPa with different amplitudes. The number of specimens with equal and unequal impacts is represented as D-0.6-1 and B-0.6-1, respectively, where D and B represent the equal and unequal amplitudes, respectively, and 0.6 represents the equal and unequal impact pressures. The initial impact air pressure, 1, is the test group number. There are a total of 5 test groups, and each group is cyclically impacted until failure. The details of the test protocol are shown in Table 1.

Figure 4: Granite specimen with a vertical hole.

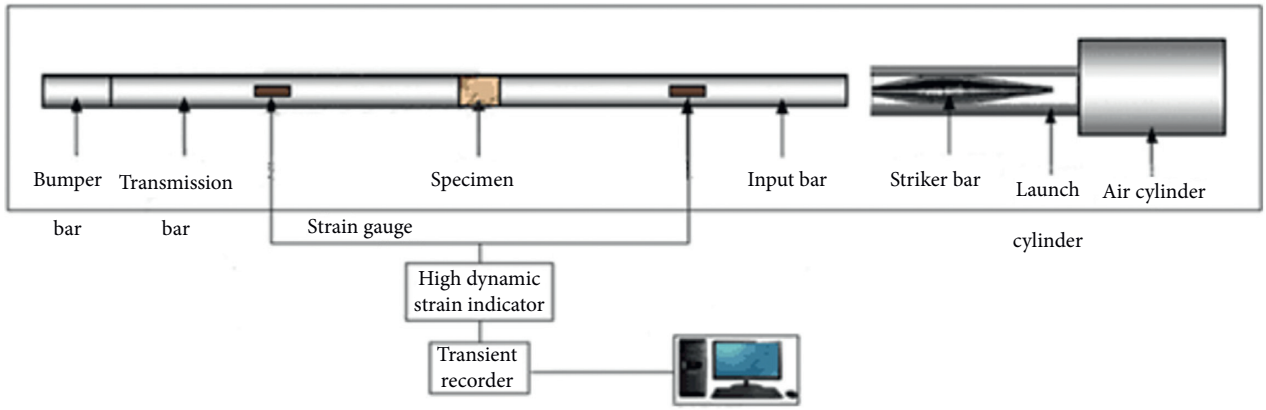

Figure 5: Schematic diagram of the SHPB test system and testing equipment [36].

Table 1: Scheme of the impact experiment.

Experimental group	Aspect ratio	Impact air pressure (MPa)
Constant-amplitude pressure shock load	2.0	0.6
	2.0	0.7
	2.0	0.8
Uneven-amplitude air pressure shock load	2.0	0.6–0.7
	2.0	0.7–0.8

3.3.2. The Procedure

(i) Before the start of the test, the incident rod and the transmission rod are closely pressed for a test punch, and the trend of the incident wave and the transmitted wave on the oscilloscope is observed to ensure that the two rods are properly connected so that the specimen can achieve stress balance during the test

(ii) During the test, butter is evenly applied to both ends of the specimen to ensure that the two ends are in good contact with the incident rod and the transmission rod since butter can reduce the impact of the friction between the rock and the rod interface during the test

(iii) The position of the punch in the transmitting cavity is adjusted, and it is confirmed that the position is fixed each time to equalize the incident stress wave on the incident rod

(iv) The cylinder air pressure is changed to the planned set value, and the strain gauge and oscilloscope are turned on for data recording

4. Results and Analysis

4.1. Experimental Results. According to the one-dimensional stress wave theory and the law of the conservation of energy, the incident energy $\sigma_I(t)$, reflected wave $\sigma_R(t)$, and transmitted wave $\sigma_R(t)$ recorded on the DL-750 oscilloscope are used to calculate the incident energy during cyclic impact, reflection energy, transmission energy, average strain rate, and absorbed energy per unit volume, and then the degree of damage after each impact is obtained from equation (11). Due to space limitations, Table 2 only lists the results of some test specimens. Table 2 shows that with the increase in the number of cyclic impacts, the absorbed energy per unit volume and the average strain rate of the specimen gradually increase and the wave impedance gradually decreases. The dynamic peak

Table 2: Experimental results for some granite specimens under cyclical impact loads.

Specimen number	Impact air pressure (MPa)	Number of impacts	Wave impedance (MPa/s)	Incident energy (J)	Absorption energy per unit volume (J/cm^3)	Average strain rate (s^{-1})	Dynamic peak stress (MPa)
D-0.6-2	0.6	1	127.83	78.83	0.123	24.82	113.89
		2	108.55	80.05	0.152	30.86	85.39
		3	103.68	81.86	0.156	31.14	83.09
		4	99.36	81.88	0.156	30.23	88.63
		5	93.57	75.76	0.165	32.41	82.68
		6	72.72	77.87	0.206	38.02	59.37
D-0.7-3	0.7	1	125.04	123.47	0.186	30.84	131.63
		2	111.38	126.64	0.194	31.73	129.46
		3	95.88	123.04	0.263	39.37	95.58
		4	63.03	126.11	0.291	42.09	76.46
D-0.8-3	0.8	1	117.34	163.35	0.255	36.76	150.38
		2	88.36	162.27	0.311	41.75	137.02
		3	41.09	157.22	0.415	51.67	98.94
B-0.6-1	0.6–0.7	1	123.41	83.23	0.165	27.15	74.90
		2	34.77	127.49	0.276	35.51	118.77
B-0.7-3	0.7–0.8	1	118.23	113.31	0.157	28.61	101.65
		2	26.87	152.21	0.330	39.83	129.68

stress decreases gradually during equal-amplitude impact generally, but it increases during uneven-amplitude impact.

4.2. Damage Evolution Characteristic Curve. Figure 6 shows the relationship between the degree of damage and the number of impacts during cyclic loading. From the analysis of the graph, it can be seen that the damage accumulation of rock specimens with vertical holes increases as the number of impacts increases, and basically, as the impact load increases, the cumulative damage growth rate of its cyclic impact also increases. The number of impacts gradually decreases. Due to the existence of hole defects, a large number of cracks are generated near the hole wall during the impact process, and the rock itself contains initial cracks. The analysis shows that each group of specimens has a larger damage value after the first impact. The range of this value is 0.2~0.3. Subsequent shocks are affected by the magnitude and change in the pressure of the shock, and the change law of the damage is also different.

The damage accumulation of the granite specimen D-0.6-2 slowly increased during the second to fourth impacts. At this stage, the curve change trend was relatively gentle, and the dynamic peak stress and the average strain rate were basically unchanged. After the impact, initial microcracks and pore compaction appeared inside the rock, while the crack initiation and propagation process around the hole continued, reflecting the overall situation that the deformation characteristics were relatively stable, and the rock samples had good ductility characteristics. The degree of damage to the test specimen continued to increase. At this stage, cracks occurred in various directions in the rock and around the hole. Cracks with an inclination greater than the internal friction angle began to rapidly expand and penetrate due to the insufficient bearing capacity of the specimen. The yield area of the cross section of the rock continued to increase until the specimen was damaged. The damage

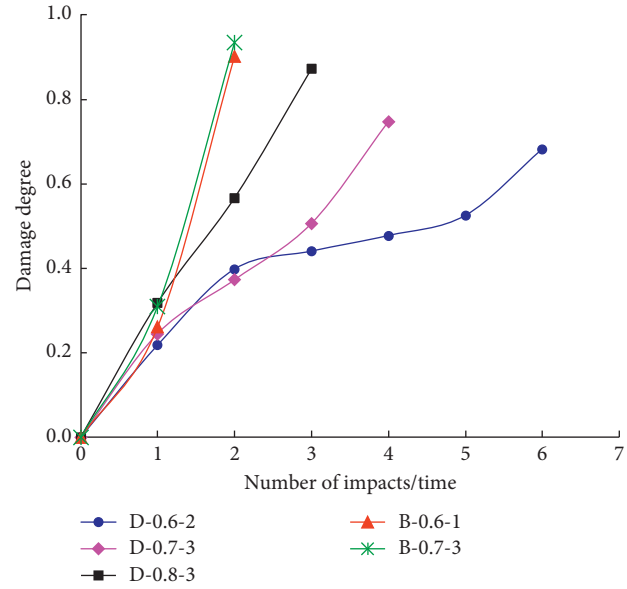

Figure 6: Relationship between the damage degree and number of impacts.

evolution curve for the entire process includes the process from the initial stage to the low-speed stage and the acceleration stage, which can better characterize the fatigue mechanical properties of rocks under cyclic impact. Comparing specimen D-0.6-2 and specimen D-0.7-3, due to the increase in the impact gas pressure, the damage accumulation rate in the whole process is accelerated, the number of impacts is reduced, the low-speed stage of the rock damage evolution disappears, and the dynamic peak stress gradually decreases with the number of impacts. When the dynamic load is further increased to an impact pressure of 0.8 MPa, the damage accumulation rate of specimen D-0.8-3 is much greater than that of the previous two groups, the degree of

damage increases approximately linearly, the number of impacts decreases, and the rock brittleness increases. The damage during the initial and final failure stages is also larger than that of the previous two groups. It can be considered that this result occurs because the specimen exhibited more cracks in the first impact stage, and the final impact specimen had a higher degree of fragmentation.

Both specimens B-0.6-1 and B-0.7-3, under different amplitude impacts, were destroyed after two impacts. The phenomenon occurred because the damage was small under the first impact, and the second incident was caused by the increase in the air pressure. The stress wave amplitude and strain rate increase accordingly, the impact damage accumulation sharply increases, and the relationship between the degree of damage and the number of impacts exponentially increases. Compared with that of specimen D-0.6-2 and specimen D-0.7-3, the degree of damage to the rock at this time exhibits a more dramatic, sudden increase, and the final degree of damage is also more severe. Compared with those following the equal-amplitude impact, the mechanical properties of the specimens with unequal-amplitude impact deteriorate faster, and the rock exhibits significant brittle failure characteristics. The reasons for this phenomenon will be discussed in conjunction with the energy dissipation.

Except for specimen D-0.6-2, with an impact pressure of 0.6 MPa, the peak stress value of the rock significantly decreases with an increase in the number of impacts. The crack growth rate of the vertical hole granite is greater than the strength capacity of the rock structure required after compaction. At this time, the magnitude of the impact load exceeds the critical value of the dynamic load that disappears at the low-speed stage. During the multiple impacts of the specimen, the internal cracks continue to sprout, expand, and penetrate, resulting in increased specimen damage and reduced load carrying capacity.

4.3. Analysis of the Average Strain Rate and Damage Characteristics. The damage model deduced from the continuous condition of the interface shows that the degree of damage D is a function of the ratio of the transmitted wave $\sigma_T(t)$ to the incident wave $\sigma_I(t)$, which represents the gradual weakening of the cohesion in the rock and the degree of volume unit failure. Assuming that the rock stress is uniform and without attenuation, the strain rate $\dot{\varepsilon}$ is a function of the reflected wave $\sigma_R(t)$ in the two-wave method, which represents the rate of change of the rock strain. Therefore, there is a certain degree of damage D and strain rate $\dot{\varepsilon}$ during impact contact. Figure 7 shows the change in the degree of damage with the average strain rate under different impact air pressures of the same amplitude impact. The analysis shows that when the impact gas pressure is constant, the damage to the specimen increases with the increase in the average strain rate, which indicates that as the strain rate increases, the degree of structural deterioration caused by crack initiation and propagation in the rock is more serious. Increasing the impact air pressure causes the specimen damage accumulation curve as a whole to shift to the right, and the size of the damage under a high strain rate increases, which shows that the increase in rock damage under high pressure impact is

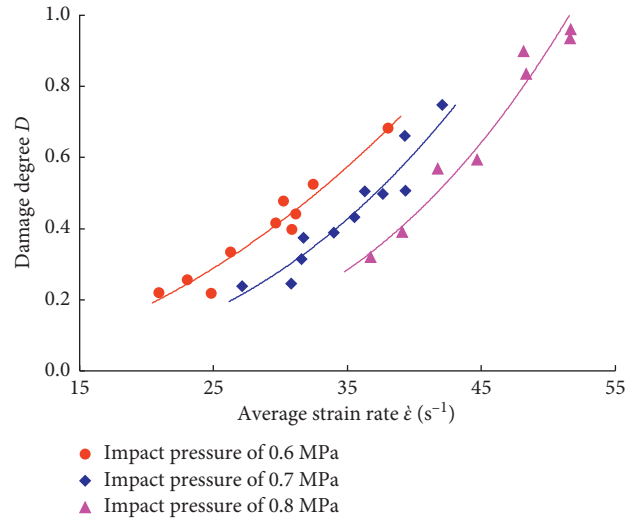

Figure 7: Relationship between the degree of damage and the average strain rate under different pressures of equal amplitude.

greater as the average strain rate increases. Therefore, it can be considered that the increase in the impact pressure weakens the impact strength of granite and accelerates the damage evolution rate of the internal structure under impact loading, and the larger the impact pressure within a certain range is, the faster the damage evolution rate of the specimen is.

To investigate the relationship between the rock damage and the average strain rate under more impact pressures, the power function $D = \alpha\dot{\varepsilon}^{\beta}$ was used to fit the data in Figure 6 to obtain the relationship between the degree of damage and the average strain rate at different impact pressures:

$$\begin{aligned} &P_n = 0.6\,\text{MPa}, \quad D = 4.01 \times 10^{-4}\dot{\varepsilon}^{2.0439}, \quad R^2 = 0.913,\\ &P_n = 0.7\,\text{MPa}, \quad D = 2.92 \times 10^{-5}\dot{\varepsilon}^{2.6972}, \quad R^2 = 0.910,\\ &P_n = 0.8\,\text{MPa}, \quad D = 2.73 \times 10^{-6}\dot{\varepsilon}^{3.2490}, \quad R^2 = 0.965. \end{aligned} \tag{12}$$

The impact pressure is fitted to the parameters α and β to obtain the following equation:

$$\begin{cases} \alpha = 1.22 \times 10^3 \cdot e^{-24.9467P_n}, & R^2 = 0.998,\\ \beta = 6.03P_n - 1.5544, & R^2 = 0.997. \end{cases} \tag{13}$$

By substituting equation (13) into the power function $D = \alpha\dot{\varepsilon}^{\beta}$, we can obtain the expression for the relationship between the degree of damage to the rock and the impact pressure and the average strain rate:

$$D = \left(1.22 \times 10^3 \cdot e^{-24.9467P_n}\right)\dot{\varepsilon}^{6.03-1.5544}. \tag{14}$$

Figure 8 shows the comparison between the test result fitting and the equation theoretical curve at $P_n = 0.7$ MPa. It can be seen from the figure that the fitted curve and the experimental curve are almost coincident, there are only slight differences in the high-strain section, and the overall trend of the numerical changes is the same. The average strain rate-degree of damage curve calculated by the theoretical equation is very similar to the experimental fit curve. Using equation (14), the relationship between the degree of

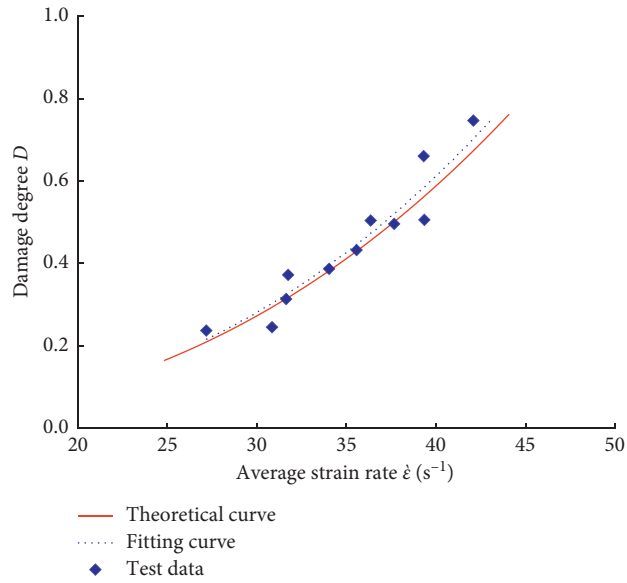

Figure 8: Relationship between the average strain rate and the degree of damage for $P_n = 0.7$ MPa.

damage and the average strain rate under other pressure shocks can be calculated, and the relationship between the development rate of internal defects and the degree of structural damage when the load is applied on the granite with different impacts can be obtained. Because the experimental data of the unequal-amplitude experimental group are small and the relationship between the strain rate and damage evolution under alternating impact pressure is relatively complicated, the theoretical equation for such cases is not discussed.

4.4. Relationship between the Absorbed Energy per Unit Volume and Strain Rate. Figure 9 shows the relationship between the absorbed energy per unit volume and the average strain rate during the cyclic impact of the specimen under constant and unequal pressure. It can be seen from the figure that under the action of equal- and unequal-amplitude air pressure shocks, the absorption energy per unit volume of the rock increases linearly with the increase in the average strain rate.

Figure 9(a) shows the fitting of the relationship between the absorbed energy per unit volume and the average strain rate under different air pressures of equal-amplitude impact. As the increase in the impact air pressure leads to an increase in the punch speed, the average strain rate generated by the specimen also increases overall. The slope of the linear fitting is greater under high pressure, and the absorption energy per unit volume increases rapidly with the strain rate. On the other hand, the slope of the linear fitting under low pressure is smaller, and the absorption energy per unit volume increases slowly with the strain rate. By examining the impact of different impact modes on the law of rock damage, as shown in Figures 9(b) and 9(c), when the average strain rate is small, the energy values are not very different, and under a high average strain rate, the energy absorption efficiency of the specimen under the impact of unequal amplitude is stronger than that under equal amplitude, which indicates that the energy absorption efficiency of the specimen is improved under the impact of high air pressure.

The analysis shows that under the action of a large impact load, the development rate of internal defects in the rock will gradually increase. At this time, the looser the specimen is, the smaller the wave impedance value is and the higher the degree of damage is. If the same average strain rate occurs, a specimen impacted by a high pressure must absorb more energy to do work on more crack slip surfaces, so the slope of the absorbed energy per unit volume and the average strain rate during cyclic impact will increase with the increase in the impact pressure.

4.5. Relationship between the Number of Impacts and Specific Energy Absorption. To explore the relationship between the number of impacts of rock and the damage under cyclic impact loading, the cumulative specific energy absorption value ϑ is defined as the accumulated energy absorbed per unit volume of the specimen during cyclic impact:

$$\vartheta = \sum_{i=0}^{n} E_{V(i)}, \tag{15}$$

where ϑ is the cumulative specific energy absorption value, $E_{V(i)}$ is the absorbed energy per unit volume generated by the i-th impact of the specimen, and n is the number of impacts of the cyclic load. The relationship between the cumulative specific energy absorption value of the rock and the number of impact loads can be obtained from the test results and equation (15). Figure 10 shows the relationship between the cumulative specific energy absorption of rock and the number of impacts under different impact pressures and impact modes.

With constant amplitude impact, as the pressure of the impact gas increases, the rate of increase of the specific energy of the specimen increases and the number of impacts decreases accordingly. The last impact incident energy is mainly used for specimen failure [37], resulting in a

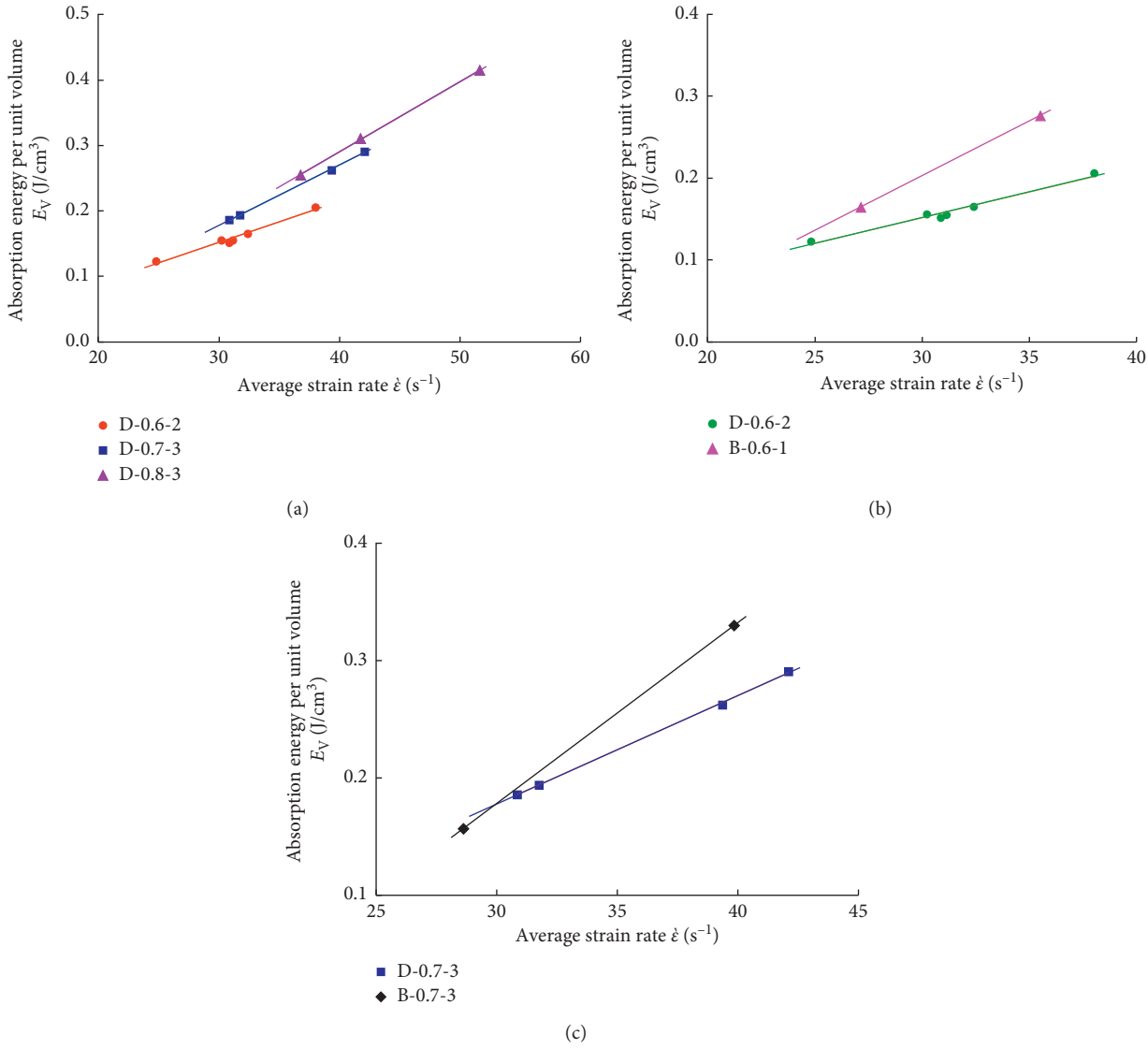

Figure 9: Variation laws of the absorbed energy per unit volume with the strain rate. (a) Pressure shocks of 0.6 MPa, 0.7 MPa, and 0.8 MPa. (b) Pressure shocks of 0.6 MPa and 0.6 MPa-0.7 MPa. (c) Pressure shocks of 0.7 MPa and 0.7 MPa-0.8 MPa.

relatively large absorbed energy of the specimen. This test showed a significant increase in the last absorption energy under high pressure impact. Specimen D-0.8-3 showed an increase by 50.39% and 29.89% in the last unit volume compared to that of specimens D-0.6-2 and D-0.7-3, respectively. Figure 10 shows the failure mode of a granite specimen with holes under constant amplitude impact. At an impact pressure of 0.6 MPa, specimen D-0.6-2 undergoes lateral tensile failure near the middle, with some spalling at the edges; at 0.7 MPa, the failure degree of specimen D-0.7-3 is incomplete. The secondary rock block undergoes lateral stretching and axial splitting along the diameter section of the hole, and the surface of the main rock block undergoes longitudinal tensile cracking that extends to the edge of the hole with a circular cross section; under the impact of 0.8 MPa, specimen D-0.8-3 breaks into three main blocks, there is a lateral stretching zone and an axial splitting zone, and the flaking and fragmentation of the rock edge is more severe.

For the case of unequal-amplitude impact, the number of impacts of the rock is significantly reduced compared to the number of equal-amplitude impacts, and the accumulated specific energy at the time of the final failure is also greatly reduced. Compared with specimen D-0.6-2 and specimen D-0.7-3, specimen B-0.6-1 and specimen B-0.7-3 both produced a greater accumulated specific energy due to the subsequent increase in the impact gas pressure. The growth rate increased by 25.45% and 11.85%, respectively. The failure morphology of the rock specimen under unequal-amplitude impact is shown in Figure 11. The failure mode of specimen B-0.6-1 under pressures of 0.6-0.7 MPa is a combination of lateral stretching and axial splitting failure, and under a pressure of 0.8 MPa, specimen B-0.7-3 exhibits a complete axial splitting failure

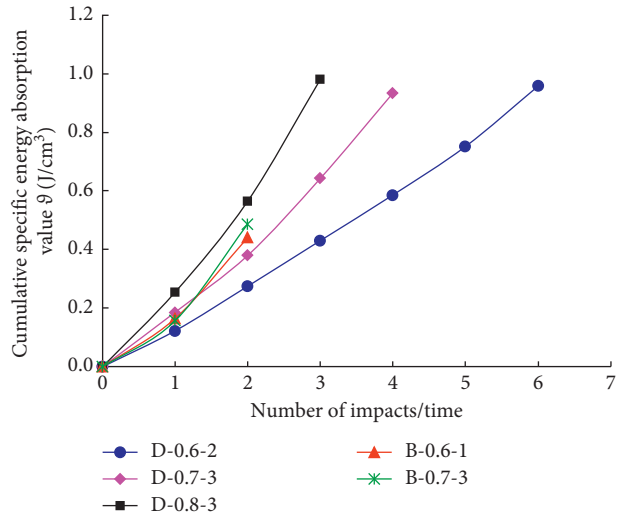

Figure 10: Relationship between the value of the cumulative specific energy and time of the impact loads.

Figure 11: Fracture failure morphology of granite specimens with a vertical hole under different impact pressures of equal-amplitude impact.

mode, and rock blocks spall and break at both ends of the specimen.

5. Discussion

With the increase in the impact pressure and the change in the impact mode, the failure mode of the rock undergoes a transformation from lateral tensile failure to lateral tensile-axial splitting combination and axial splitting failure and is affected by the size effect of granite. The degree of the final fracture of the specimen is not serious. The explosion stress wave reflection tensile theory assumes that rock failure is caused by the stress wave in the rock, forming a reflected tensile wave after the free surface is reflected, and the tensile stress in the rock is greater than its tensile strength. When the stress wave is transmitted from the incident rod to the specimen, a short elastic deformation displacement difference occurs in the interface area due to the difference in the elastic modulus. During the entire impact process, there are multiple transreflective stress waves. Each time the stress wave is transmitted to the interface between the specimen and the rod, a relative displacement will be produced. With the increase in the number of times, the stress wave propagates in the specimen, the microcracks will propagate and penetrate in succession, resulting in the enhanced deformation capacity of the rock, and the relative displacement generated each time will gradually increase. In addition, due to the lack of axial compression constraints, the transmission rod will undergo a certain displacement after being subjected to several transmission stress waves. At a certain reflection and reflection stage, a side of the specimen will form a hollow surface with the elastic rod and generate reflected tensile waves [38]. The existence of holes intensifies the crack propagation rate in each reflective process and reduces the net cross-sectional area of the active surface, which results in the lateral tensile failure of the rock. Increased impact air pressure leads to the initiation of the concentrated tensile stress generated near the hole wall, causing the split-through surface to develop in the axial direction. Under the high pressure of unequal-amplitude impact, the stress concentration around the hole is further intensified. Before the formation of hysteresis, the test specimen will split and break because the tensile stress around the hole exceeds its tensile strength. The excessive local compressive stress causes a certain crushing.

According to the theoretical analysis, during microcrack initiation and propagation, slippage will inevitably occur. As the cyclic impact progresses, the penetration crack surface

Figure 12: Fracture failure morphology of the granite specimen with a vertical hole under different impact pressures with unequal-amplitude impact.

will continue to increase. At this time, the work required to overcome the friction of the section slip will incrementally increase. The absorbed energy per unit volume of the rock will also increase, causing the cumulative specific energy absorption value to gradually increase, while the damage accumulation of the rock will increase one after another. In this experiment, with the increase in the equal-pressure impact gas pressure, the degree of fracture and the area of fracture of the specimen increase correspondingly and the impact strength also weakens successively. Under unequal-amplitude impact, the specimen exhibits a more severe degree of fragmentation at a lower cumulative specific energy absorption value. Compared with that of equal-amplitude impact, the impact resistance of the specimen under unequal-amplitude impact is greatly reduced and the damage evolution is more severe. The high-pressure shock aggravates the propagation rate of the microdefects inside the test specimen after the low-pressure shock, and the stress concentration around the hole initiates more cracks. When most of the cracks have not yet initiated and propagated, the test specimen A section has been loaded with a low capacity, and a large crack density expands, penetrates, and breaks. According to Figures 11 and 12, the through surface usually forms along the section where the diameter of the hole is located. Therefore, in engineering practice, when the rock is subjected to large dynamic loads and varying dynamic loads, construction personnel should pay attention to locations with defects and take corresponding measures to support and strengthen the surrounding rocks [39–41].

6. Conclusions

This paper proposed a damage constitutive model defined by wave impedance, which can quantify the damage degree of the granite with a hole paralleled with the load direction, and provided a new method for predicting the damage process of confining pressure in engineering practice. Through the constitutive model, it can be found that the degree of damage and the change rate of cumulative specific energy absorption value of the specimens accelerated, and the impact strength significantly decreases as the number of impacts increases. During the experiment, the specimens with holes showed significant brittle failure characteristics, and the failure mode underwent the transformation of transverse tensile failure to transverse tension-axial splitting combination and axial splitting failure. Through the analysis of rock energy changes and rock failure patterns during cyclic impact, it will be helpful to predict and control the fracture caused by local stress concentration during excavation, thus can reduce the cost of support and reinforcement in excavation and improve the stability of the surrounding rocks.

Data Availability

The data used to support the findings of this study are available from the corresponding author upon request.

Conflicts of Interest

The authors declare that they have no known conflicts of interest that could influence the work reported in this paper.

Authors' Contributions

Bing Dai was responsible for methodology; Li Chen conceptualized the study; Yakun Tian was involved in investigation and data curation; Xinyao Luo wrote the original draft; Ying Chen was responsible for resources and writing (reviewing and editing); Zhijun Zhang supervised the study; Qiwei Shan was involved in validation and visualization.

Acknowledgments

This study was conducted under the joint grant of the National Natural Science Foundation of China (no. 51804163) and the China Postdoctoral Science Foundation (2018M642678).

References

[1] P.-X. Li, X.-T. Feng, G.-L. Feng, Y.-X. Xiao, and B.-R. Chen, "Rockburst and microseismic characteristics around lithological interfaces under different excavation directions in deep tunnels," *Engineering Geology*, vol. 260, Article ID 105209, 2019.

[2] X. Xu, M. He, C. Zhu, Y. Lin, and C. Cao, "A new calculation model of blasting dam-age degree-based on fractal and tie rod damage theory," *Engineering Fracture Mechanics*, vol. 220, 2019.

[3] X. B. Li, T. S. Lok, and J. Zhao, "Dynamic characteristics of granite subjected to intermediate loading rate," *Rock Mechanics and Rock Engineering*, vol. 38, no. 1, pp. 21–39, 2005.

[4] X. Luo, N. Jiang, M. Wang, and Y. Xu, "Response of leptynite subjected to repeated impact loading," *Rock Mechanics and Rock Engineering*, vol. 49, no. 10, pp. 4137–4141, 2016.

[5] J. Fan, J. Chen, D. Jiang, S. Ren, and J. Wu, "Fatigue properties of rock salt subjected to interval cyclic pressure," *International Journal of Fatigue*, vol. 90, pp. 109–115, 2016.

[6] S. H. Li, W. C. Zhu, L. L. Niu, M. Yu, and C. F. Chen, "Dynamic characteristics of green sandstone subjected to repetitive impact loading: phenomena and mechanisms," *Rock Mechanics and Rock Engineering*, vol. 51, no. 6, pp. 1921–1936, 2018.

[7] J. J. Zhu, X. B. Li, F. Q. Gong, and S. M. Wang, "Dynamic characteristics and damage model for rock under uniaxial cyclic impact compressive loads," *Chinese Journal of Geotechnical Engineering*, vol. 35, no. 3, pp. 531–539, 2013.

[8] F.-Q. Gong, X.-F. Si, X.-B. Li, and S.-Y. Wang, "Dynamic triaxial compression tests on sandstone at high strain rates and low confining pressures with split Hopkinson pressure bar," *International Journal of Rock Mechanics and Mining Sciences*, vol. 113, pp. 211–219, 2019.

[9] R.-H. Shu, T.-B. Yin, X.-B. Li, Z.-Q. Yin, and L.-Z. Tang, "Effect of thermal treatment on energy dissipation of granite under cyclic impact loading," *Transactions of Nonferrous Metals Society of China*, vol. 29, no. 2, pp. 385–396, 2019.

[10] K. Peng, J. Zhou, Q. Zou, and F. Yan, "Deformation characteristics of sandstones during cyclic loading and unloading with varying lower limits of stress under different confining pressures," *International Journal of Fatigue*, vol. 127, pp. 82–100, 2019.

[11] K. Peng, J. Zhou, Q. Zou, and X. Song, "Effect of loading frequency on the deformation behaviours of sandstones subjected to cyclic loads and its underlying mechanism," *International Journal of Fatigue*, vol. 131, Article ID 105349, 2020.

[12] M. Tao, H. Zhao, A. Momeni, Y. Wang, and W. Cao, "Fracture failure analysis of elliptical hole bored granodiorite rocks under impact loads," *Theoretical and Applied Fracture Mechanics*, vol. 107, Article ID 102516, 2020.

[13] B. Dai and Y. Chen, "A novel approach for predicting the height of the water-flow fracture zone in undersea safety mining," *Remote Sensing*, vol. 12, no. 3, p. 358, 2020.

[14] Z.-l. Zhou, Y. Zhao, Y.-h. Jiang, Y. Zou, X. Cai, and D.-y. Li, "Dynamic behavior of rock during its post failure stage in shpb tests," *Transactions of Nonferrous Metals Society of China*, vol. 27, no. 1, pp. 184–196, 2017.

[15] X. Li, Z. Zhou, T.-S. Lok, L. Hong, and T. Yin, "Innovative testing technique of rock subjected to coupled static and dynamic loads," *International Journal of Rock Mechanics and Mining Sciences*, vol. 45, no. 5, pp. 739–748, 2008.

[16] X. Li, T. Zhou, and D. Li, "Dynamic strength and fracturing behavior of single-flawed prismatic marble specimens under impact loading with a split-hopkinson pressure bar," *Rock Mechanics and Rock Engineering*, vol. 50, no. 1, pp. 29–44, 2017.

[17] M. Tao, M. Ao, W. Cao, X. Li, and F. Gong, "Dynamic response of pre-stressed rock with a circular cavity subject to transient loading," *International Journal of Rock Mechanics and Mining Sciences*, vol. 99, pp. 1–8, 2017.

[18] D. Liu, D. Li, F. Zhao, and C. Wang, "Fragmentation characteristics analysis of sandstone fragments based on impact rockburst test," *Journal of Rock Mechanics and Geotechnical Engineering*, vol. 6, no. 3, pp. 251–256, 2014.

[19] H. Wu, G. Zhao, W. Liang, and E. Wang, "Dynamic mechanical characteristics and failure modes of sandstone with artificial surface cracks," *Journal of Central South University (Science and Technology)*, vol. 50, no. 02, pp. 106–115, 2019.

[20] D. Han, K. Li, and J. Meng, "Evolution of nonlinear elasticity and crack damage of rock joint under cyclic tension," *International Journal of Rock Mechanics and Mining Sciences*, vol. 128, Article ID 104286, 2020.

[21] Q. Meng, M. Zhang, L. Han, H. Pu, and Y. Chen, "Acoustic emission characteristics of red sandstone specimens under uniaxial cyclic loading and unloading compression," *Rock Mechanics and Rock Engineering*, vol. 51, no. 4, pp. 969–988, 2018.

[22] D. Zhu, Y. Wu, Z. Liu, X. Dong, and J. Yu, "Failure mechanism and safety control strategy for laminated roof of wide-span roadway," *Engineering Failure Analysis*, vol. 111, Article ID 104489, 2020.

[23] Q. Zheng, E. Liu, P. Sun, M. Liu, and D. Yu, "Dynamic and damage properties of artificial jointed rock samples subjected to cyclic triaxial loading at various frequencies," *International Journal of Rock Mechanics and Mining Sciences*, vol. 128, Article ID 104243, 2020.

[24] Q. Meng, M. Zhang, L. Han, H. Pu, and T. Nie, "Effects of acoustic emission and energy evolution of rock specimens under the uniaxial cyclic loading and unloading compression," *Rock Mechanics and Rock Engineering*, vol. 49, no. 10, pp. 3873–3886, 2016.

[25] H. Wu, G. Zhao, and W. Liang, "Mechanical properties and fracture characteristics of pre-holed rocks subjected to uniaxial loading: a comparative analysis of five hole shapes," *Theoretical and Applied Fracture Mechanics*, vol. 105, Article ID 102433, 2020.

[26] K. Chen, M. Tang, and Z. Guo, "Comparative study on three-dimensional conventional and modified statistical damage constitutive models," *Multiscale and Multidisciplinary Modeling, Experiments and Design*, vol. 2, no. 4, pp. 259–267, 2019.

[27] Z. Zhou, L. Tan, W. Cao, Z. Zhou, and X. Cai, "Fracture evolution and failure behaviour of marble specimens containing rectangular cavities under uniaxial loading," *Engineering Fracture Mechanics*, vol. 184, pp. 183–201, 2017.

[28] L. Scholtès and F.-V. Donzé, "Modelling progressive failure in fractured rock masses using a 3d discrete element method," *International Journal of Rock Mechanics and Mining Sciences*, vol. 52, pp. 18–30, 2012.

[29] Y. Matvienko, V. Pisarev, and S. Eleonsky, "The effect of low-cycle fatigue parameters on damage accumulation near a hole," *Engineering Failure Analysis*, vol. 106, Article ID 104175, 2019.

[30] D. Li, Q. Zhu, and X. Li, "Research on the effect of cavity shapes for the progressive failure and mechanical behavior of marb," *Journal of Underground Space and Engineering*, vol. 14, no. 1, pp. 58–66, 2008.

[31] C. Zhang, J. Tang, J. Teng, and C. Li, "Experimental study of influences of pore number and pore size on mechanical properties of marble," *Rock and Soil Mechanics*, vol. 38, no. S2, pp. 41–50, 2017.

[32] J. Qiu, L. Luo, X. Li, D. Li, Y. Chen, and Y. Luo, "Numerical investigation on the tensile fracturing behavior of rock-shotcrete interface based on discrete element method," *International Journal of Mining Science and Technology*, 2020.

[33] J. Jiefang, L. Xibing, Y. Zhiqiang, and Z. Yang, "A method for defining rock damage variable by wave impedance under

cyclic impact loadings," *Rock and Soil Mechanics*, vol. 32, no. 5, pp. 1385–1393, 2011.

[34] D. Ai, Y. Zhao, Q. Wang, and C. Li, "Crack propagation and dynamic properties of coal under SHPB impact loading: experimental investigation and numerical simulation," *Theoretical and Applied Fracture Mechanics*, vol. 105, Article ID 102393, 2020.

[35] J. G. Cai and J. Zhao, "Effects of multiple parallel fractures on apparent attenuation of stress waves in rock masses," *International Journal of Rock Mechanics and Mining Sciences*, vol. 37, no. 4, pp. 661–682, 2000.

[36] F.-Q. Gong and G.-F. Zhao, "Dynamic indirect tensile strength of sandstone under different loading rates," *Rock Mechanics and Rock Engineering*, vol. 47, no. 6, pp. 2271–2278, 2014.

[37] L. Xibing, G. Fengqiang, Z. Jian, G. Ke, and Y. Tubing, "Test study of impact failure of rock subjected to one-dimensional coupled static and dynamic loads," *Chinese Journal of Rock Mechanics and Engineering*, vol. 29, no. 02, pp. 251–260, 2010.

[38] W. Dang, H. Konietzky, T. Frühwirt, and M. Herbst, "Cyclic frictional responses of planar joints under cyclic normal load conditions: laboratory tests and numerical simulations," *Rock Mechanics and Rock Engineering*, vol. 53, no. 1, pp. 337–364, 2020.

[39] W. Dang, H. W. Wu, and J. Qian, "Effect of shear-induced aperture evolution on fluid flow in rock fractures," *Computers and Geotechnics*, vol. 114, Article ID 103152, 2019.

[40] W. Dang, L. H. Konietzky, and T. Frühwirt, "Velocity-frequency-amplitude-dependent frictional resistance of planar joints under dynamic normal load (DNL) conditions," *Tunnelling and Underground Space Technology*, vol. 79, no. 9, pp. 27–34, 2018.

[41] Y. Luo, F. Q. Gong, X. B. Li, and S. Y. Wang, "Experimental simulation investigation of influence of depth on spalling characteristics in circular hard rock tunnel," *Journal of Central South University*, vol. 27, no. 3, pp. 891–910, 2020.